Korean J. Chem. Eng., 37(6), 1071-1085 (2020)
DOI: 10.1007/s11814-020-0512-7

pISSN: 0256-1115
eISSN: 1975-7220

Photocatalytic degradation of methylene blue using three-dimensional porous graphene-titania microparticles under UV light

Young-Sang Cho†, Hyeong Jin Lee, and Sohyeon Sung

Department of Chemical Engineering and Biotechnology, Korea Polytechnic University,
237 Sangidaehak-ro, Siheung-si, Gyeonggi-do 15073, Korea
(*Received 29 October 2019 • accepted 8 February 2020*)

Abstract−Porous graphene and graphene-silica microparticles containing titania nanoparticles were synthesized by emulsion-assisted self-assembly for the photocatalytic decomposition of methylene blue in an aqueous medium. After the mixed dispersion of graphene nanosheets and titania nanoparticles with or without silicic acid was prepared, the complex fluid was emulsified in a continuous oil phase to form tiny droplets that act as micro-reactors for the synthesis of porous photocatalytic particles, the morphology of which was three-dimensional spherical shapes with a number of irregular-shaped macropores. The three dimensional conductive graphene scaffolds greatly enhanced the photocatalytic activity of the porous particles due to the suppression of the recombination of electron-hole pairs generated from titania under UV light irradiation, and adsorption of dye molecules on graphene-silica scaffolds caused rapid removal of aqueous contaminants. Unlike previous reports, the kinetics of the photocatalytic decomposition reaction could not be explained by Langmuir-Hinshelwood kinetics, but the experimental data could be fitted well by the second- or third-order kinetics. This indicates that the removal rate of the pollutant could be enhanced by the supporting material. The removal efficiency of methylene blue was estimated as more than 95% when sufficient amount of the photocatalytic particles was used, implying that application to water treatment process will be possible.

Keywords: Porous Materials, Self-assembly, Photocatalytic Decomposition, Adsorption

INTRODUCTION

Nano-structured materials with high porosity have attracted much attention for various chemical applications such as catalytic supports, filters, and membranes [1-3]. Construction materials such as thermal insulators and sound absorbers, are also fabricated in the form of porous materials containing air voids [4-6]. For the fabrication of porous nano-structures, the self-assembly of complex fluids has been widely adopted in industries as well as laboratories, and the preparation of colloidal dispersions may open versatile and facile routes for the synthesis of porous materials with various functionalities including photocatalytic nanomaterials [7-9].

After pioneering research on water splitting phenomena by Honda and Fujishima in the 1970s, a great deal of attention has been paid to the photocatalytic purification of water and air by generating hydroxyl or oxygen radicals from water or air for the decomposition of organic contaminants [10]. Various approaches have been studied for the fabrication of photocatalysts, and the photocatalytic materials can be classified into two categories, solid films and slurries or particle suspension types [11,12]. In a slurry-type reactor, a colloidal dispersion of nanomaterials can be adopted as photocatalysts, whereas sol-gel coating or deposition of pastes on substrates can be employed to prepare film-type photocatalysts with sufficient thickness. For these approaches, the dispersions of particulate materials or ceramic precursors have been studied as raw materials, thus enabling economical synthesis of the photocatalytic system. At times, the use of nano-sized or nano-structured photocatalytic materials has been considered as more promising compared to the film-type photocatalysts, since a large surface to volume ratio is expected to enhance the photocatalytic efficiency. Nowadays, much attentions have been paid to the synthesis of nanoparticles for visible light photocatalysis using core-shell particles of various semiconducting materials such as ZnS, ZnO, CuO, and Cu_2O [13,14].

The separation of particle suspension having photocatalytic activity from aqueous medium has been considered as difficult, though secondary contamination is inevitable after wastewater treatment. In this context, film-type photocatalyst can be considered as a more beneficial approach in the field of photocatalytic oxidation of organic pollutants as well as photocatalytic water splitting for hydrogen production [15,16]. Since bandgap engineering of photocatalytic components such as graphene, chalcogenides, and carbon nitrides has been studied intensively, efficient two-dimensional photocatalytic films are developed using various materials and micro-structures [17,18]. Numerous researches on interfacial engineering of heterojunction structures of photocatalytic materials have been carried out to take advantage of charge transfer in the film [19,20].

Many researchers have sought to industrialize photocatalysts by enhancing the reaction rate of the photocatalytic decomposition of contaminants using an external light source. For this purpose, conducting nanomaterials such as metal nanoparticles have been combined with photocatalysts to suppress the recombination of electron-hole pairs generated by external light to promote the decomposition rate in a polluted medium [21-24]. However, several synthesis steps are inevitable to prepare the conducting nanomaterials

†To whom correspondence should be addressed.
E-mail: yscho78@kpu.ac.kr, yscho78@gmail.com
Copyright by The Korean Institute of Chemical Engineers.

attached to the photocatalysts, and thus further research is essential to prepare highly efficient photocatalysts by more simple fabrication methods such as a one-pot synthesis approach.

Recently, titania nanoparticles were attached to graphene nanosheets instead of metallic nanomaterials to enhance the photocatalytic decomposition of organic contaminants through chemical routes [25]. However, more facile and economic routes should be developed to enhance the electrical properties of graphene, since the stacking and aggregation of two-dimensional graphene nanosheets reduces their surface area and conductive properties. Thus, a novel strategy based on self-organization of complex fluids to prepare three-dimensional porous scaffolds containing functional nanoparticles such as titania should be developed, since a three-dimensional morphology of graphene will be beneficial for various industrial applications. By resolving this issue, commercialization of photocatalysts may be accomplished with low cost and high removal rates of organic contaminants.

Until now, colored wastewater from textile industries has been purified using activated carbon or gas bubble by adsorption mechanism [26,27]. However, this adsorption approach can be used for physical binding of dye molecules on solid particles, excluding degradation of the dye molecules to reduce chromaticity. In this study, we have combined the effect of physical adsorption and photocatalytic decomposition of methylene blue using porous graphene or graphene-silica scaffold containing TiO_2 nanoparticles as photochemically active component.

We here propose a facile fabrication scheme for three-dimensionally porous graphene or graphene-silica microparticles containing titania nanoparticles using an emulsion-assisted self-assembly process for the synthesis of highly efficient photocatalysts. To enhance the decomposition rates of organic contaminants, graphene nanosheets were adopted as a carbon source during the self-organization for macroporous frameworks without using templating materials. The kinetics of the decomposition reaction was studied from experimental data to study the deviations from Langmuir-Hinshelwood kinetics, which has been developed for conventional photocatalysts. For combining effect of adsorption and photocatalysis on removal of organic dyes, silica frameworks were attached with graphene nanosheets as supporting materials for titania nanoparticles.

EXPERIMENTAL

1. Materials

For the fabrication of porous graphene microparticles containing titania nanoparticles, an aqueous dispersion of single layer graphene nanosheets purchased from US Research Nanostructures Inc. (US 7905-30g) was used as a starting material. For the synthesis of porous graphene-silica microparticles containing titania nanoparticles, silicic acid was used as a precursor of silica, which was obtained by removing sodium ions from sodium silicate solution ($Na_2O(SiO_2)x{\cdot}xH_2O$, water glass, Sigma-Aldrich). The sodium ions were removed from water glass using an ion exchange resin (Amberlite IR 120, H^+ form) bought from Sigma-Aldrich. An aqueous dispersion of anatase titania nanoparticles was procured from Nanostructured and Amorphous Materials Inc. (#7012WJWA) and used for photocatalytic activities.

N-tetradecane (98%) was purchased from Beyond Industries Limited and used as a continuous phase for the synthesis of functional microparticles. Abil EM 90 was bought from Cosnet to be used as an emulsifier. For the tests of the photocatalytic performance, methylene blue trihydrate was used as a model contaminant and purchased from Samchun Chemicals.

2. Synthesis of Porous Graphene Microparticles Containing Titania Nanoparticles

A 2-ml aqueous dispersion of single layer graphene nanosheets (1 wt%) was mixed with a 2-ml aqueous dispersion of titania nanoparticles (15 wt%). The resulting mixture was used as a dispersed phase by emulsification using tetradecane dissolving 3 wt% of Abil EM 90 as a continuous phase. For emulsification, mechanical homogenization was carried out for 1 minute using a homogenizer (hg-15a-set-a, witeg Labortechnik GmbH). The self-assembly of the titania nanoparticles and graphene nanosheets was then carried out by heating the complex fluid system at 90 °C for 1.5 hours. The produced microparticles were washed using hexane several times to remove the continuous oil phase and dried at room temperature for at least one day, followed by calcination using a box furnace (Hantech, M13P) at 500 °C for 5 hours to fix and bind the porous microparticles and titania nanoparticles.

3. Synthesis of Graphene-silica Microparticles Containing Titania Nanoparticles

To prepare the silica precursor solution, sodium silicate was purified using an ion exchange resin to form an aqueous silicic acid solution [28]. Porous graphene-silica microparticles containing titania nanoparticles were then fabricated using a mixture of aqueous silica precursor solution, the dispersion of graphene nanosheets (1 wt%), and titania nanoparticle dispersion (15 wt%) with a volume ratio of 3 : 2 : 2. The resulting aqueous dispersion was used as a dispersed phase by emulsification, and the subsequent self-assembly was performed by heating the tiny droplets at 90 °C to fabricate porous graphene-silica microparticles containing titania nanoparticles. Finally, heat treatment at 500 °C was performed to obtain composite particles with robust strength.

4. The Photocatalytic Decomposition of Organic Contaminant from Water

Methylene blue dissolved in water was decomposed by porous microparticles containing titania nanoparticles under UV irradiation [29]. A UV-visible spectrometer was used to calibrate the concentration of methylene blue as a function of the absorbance at 666 nm to obtain a calibration graph. The aqueous mixture of methylene blue and the photocatalytic microparticles with known concentrations was then exposed under eight UV lamps (F10T8 BLB, 10 W, peak wavelength at 352 and 369 nm, Black light Blue, Sankyo Denki). Before the irradiation, a dark condition was maintained in the reaction system using a black box for 30 minutes. The concentration of methylene blue was monitored for regular time intervals as a function of UV irradiation time using a UV-visible spectrometer. Before mixing with aqueous solution of photocatalytic particles, an aqueous solution of methylene blue (0.02 g/dm^3) was prepared for typical experiments.

5. Instrumentation

The morphology of the porous microparticles was observed using a field emission scanning electron microscope (FE-SEM, Hitachi-

S4700). The X-ray diffraction peaks of porous graphene microparticles containing titania nanoparticles were measured using an HR XRD machine (Smartlab, Rigaku) from 2θ=10-80°. FT-IR spectra of the microparticles with photocatalytic functionality were obtained using a FT-IR spectrometer (Thermo Fisher Scientific co. Ltd). The UV visible spectra of aqueous methylene blue solution were measured by a UV-visible spectrophotometer (OPTIZEN, POP) during photocatalytic tests. Diffuse reflectance of the film composed of photocatalytic microparticles was measured using UV-Vis-NIR Spectrophotometer (SolidSpec-3700). TOC analysis was performed using total organic carbon analyzer (Vario TOC cube).

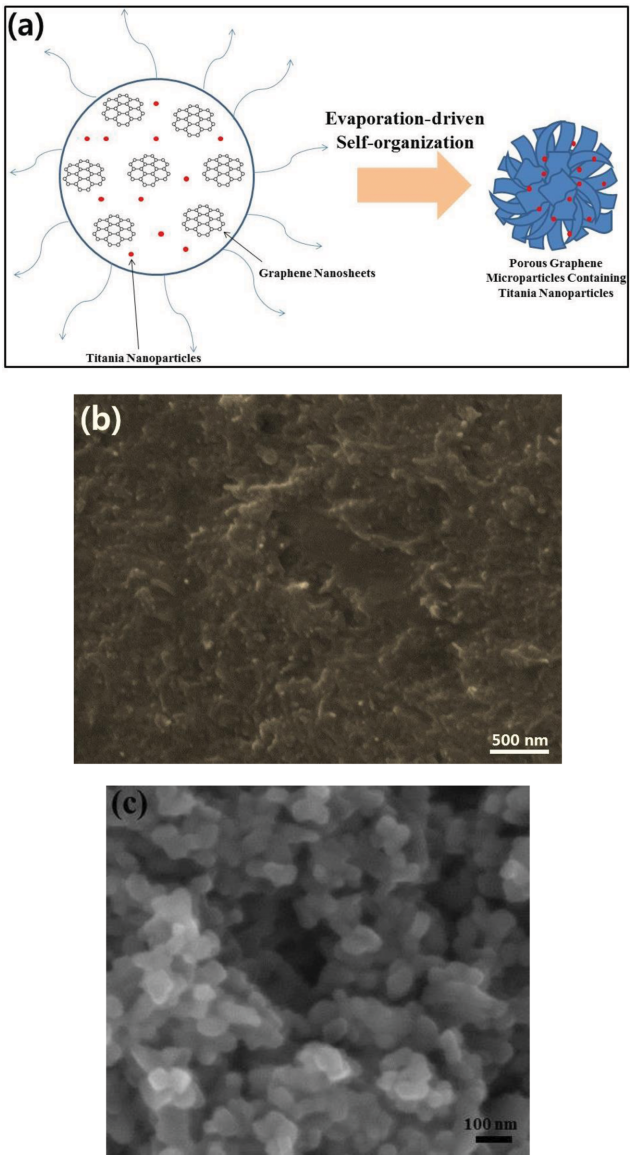


Fig. 1. (a) Schematic figure of the fabrication of the composite microparticles with graphene and titania nanoparticles by emulsion-assisted self-assembly. (b) Scanning electron microscope image of graphene nanosheets dried at room temperature. Scale bar indicates 500 nm. (c) Scanning electron microscope image of titania nanoparticles. Scale bar is 100 nm.

RESULTS AND DISCUSSION

Fig. 1(a) presents a schematic of the fabrication of porous graphene or graphene-silica microparticles containing titania nanoparticles by the suggested emulsion-assisted self-assembly scheme. In this study, single-layer graphene nanosheets were encapsulated inside emulsion droplets with titania nanoparticles after mixing the aqueous dispersion of the precursor materials. The aqueous droplets surrounded by a continuous oil phase were evaporated at elevated temperature to induce inward capillary pressure for self-organization of the dispersion of the particulate materials. Due to the crumpling and folding of the single-layer graphene nanosheets inside the droplets, the morphology of the two-dimensional graphene nanosheets was transformed to three-dimensional porous structures by self-assembly, and the bonding with titania nanoparticles became stronger after high temperature heat treatment. As displayed in the SEM image of Fig. 1(b), the natural evaporation of the dispersion medium from the dispersion of graphene nanosheets at room temperature resulted in simple stacking of the two-dimensional nanomaterials. Thus, a novel self-organization strategy is essential for the shaping of conductive nanomaterials with usable three-dimensional morphologies for practical applications. The final morphology and photocatalytic activity of the porous particles are described in this article in detail. In this study, commercial titania nanoparticles less than 100 nm displayed in the SEM image of Fig. 1(c) were self-organized with graphene nanosheets and attached to three-dimensional porous graphene microparticles by capillary force inside shrinking droplets.

1. Decomposition of Methylene Blue using Porous Graphene Microparticles Containing Titania Nanoparticles as a Photocatalyst

Porous graphene microparticles containing TiO_2 nanoparticles were fabricated from emulsion droplets as confining geometries. During heating the complex fluid system, shrinking emulsion droplets caused capillary force to self-organized graphene nanosheets and TiO_2 nanoparticles. When the mixing ratio of graphene and TiO_2 nanoparticle dispersion was 2 ml and 0.0625 ml, respectively, the resulting microstructure of the composite particles is shown in Fig. 2(a), indicating that crumpled graphene nanosheets could be produced as spheroidal microparticles. Since small amount of TiO_2 nanoparticles were added in the dispersed phase, it was difficult to recognize titania nanoparticles from the composite microparticles shown in SEM image. Average diameter of the microparticles could be estimated as 1.69 μm from the histogram in Fig. 2(b).

Fig. 2(c) presents a scanning electron microscope image of the three-dimensional porous graphene microparticles containing titania nanoparticles fabricated by the emulsion-assisted self-assembly process. The precursor mixture was prepared by mixing the dispersion of 2-ml graphene nanosheets and 2-ml titania nanoparticles. Since the original aqueous droplets were spherical, the morphologies of the resulting porous particles also were spherical, as displayed in the SEM image of Fig. 2(c). From the magnified inset SEM image of Fig. 2(c), the surface structure of the graphene particles could be observed, indicating that the microparticles had open porous surfaces originated from the assembly of several ultrathin graphene nanosheets after their folding and crumpling inside shrink-

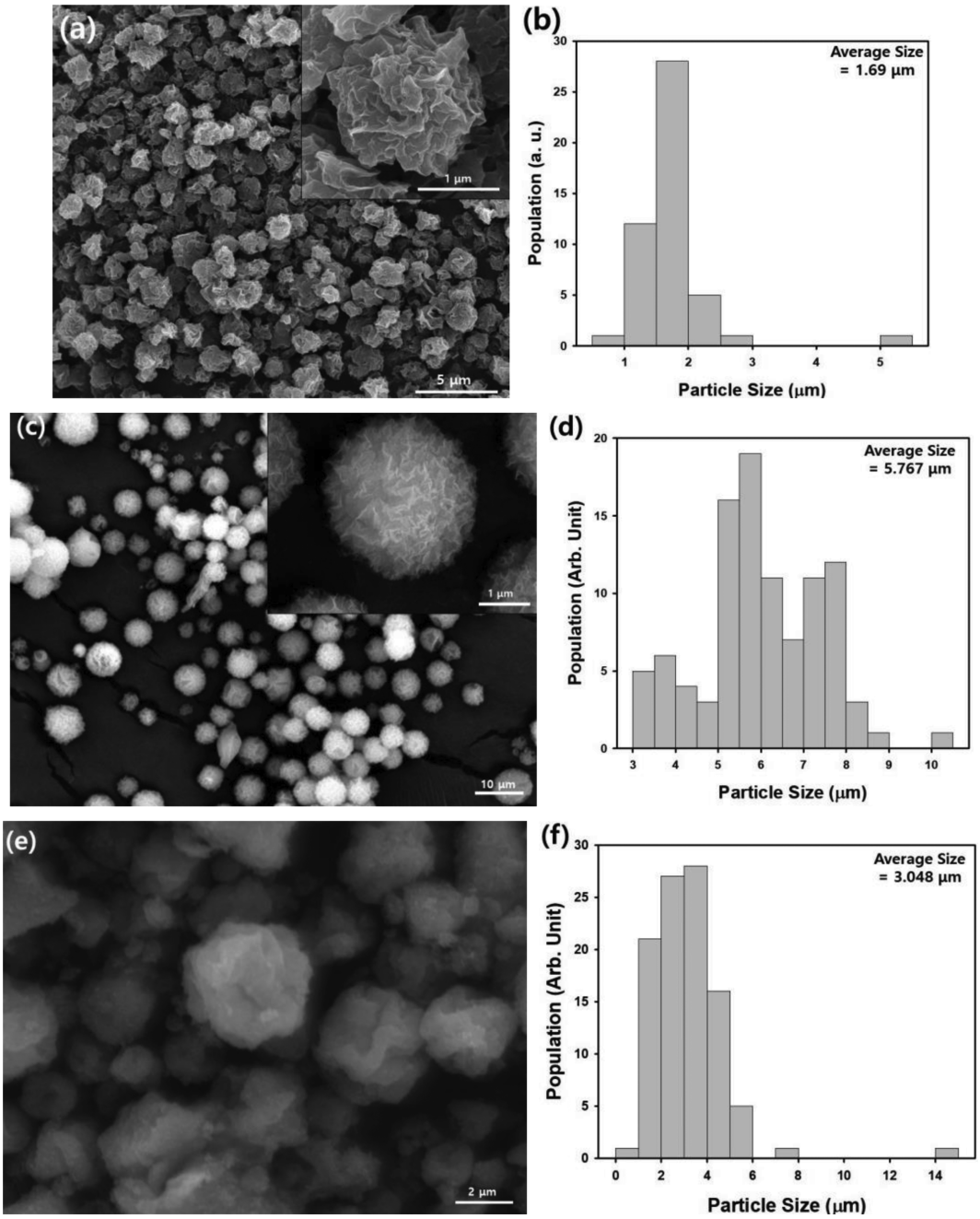


Fig. 2. (a) Scanning electron microscope image of the porous graphene microparticles containing titania nanoparticles. The precursor mixture was prepared using 2-ml graphene nanosheets and 0.0625-ml titania nano-colloid. Scale bar indicates 5 μm. The inset figure shows a magnified SEM image of the porous graphene microparticles containing titania nanoparticles. Scale bar is 1 μm. (b) The particle size distribution of the composite microparticles. (c) Scanning electron microscope image of the porous graphene microparticles containing titania nanoparticles. The precursor mixture was prepared using 2-ml graphene nanosheets and 2-ml titania nano-colloid. Scale bar indicates 10 μm. The inset figure shows a magnified SEM image of the porous graphene microparticles containing titania nanoparticles. Scale bar is 1 μm. (d) The particle size distribution of the composite microparticles. (e) Scanning electron microscope image of the porous graphene microparticles containing titania nanoparticles. The precursor mixture was prepared using 2-ml graphene nanosheets and 4-ml titania nano-colloid. Scale bar indicates 2 μm. (f) The particle size distribution of the composite microparticles.

ing droplets. The graphene nanosheets radiate from the center of the particles to form three-dimensional porous graphene balls with spherical morphologies. Since the original emulsion droplets generated by a homogenizer are polydisperse, the resulting composite microparticles also showed a relatively broad size distribution with 5.767 μm average diameter, as displayed in the histogram of Fig. 2(d).

The amount of titania nanoparticles was increased during the self-assembly process to study the change of the morphology of the porous composite particles. Fig. 2(e) presents a scanning electron microscope image of the graphene microparticles containing tita-

nia nanoparticles fabricated using a dispersion of 2-ml graphene nanosheets and 4-ml titania nanoparticles. As the amount of titania nanoparticles increased, the surface coverage of the titania nanoparticles in the composite microparticles increased, implying that the loading of the titania nanoparticles on composite microparticles could be controlled by adjusting the composition of the precursor mixture. The size distribution of the resulting particles is displayed in Fig. 2(f), and the average diameter was measured as 3.05 μm.

Previously, innovative schemes had been proposed to prepare porous graphene particles by a self-organization process of graphene nanosheets [30,31]. However, there are some drawbacks to these approaches, including that the aerosol droplets adopted as confining geometries for self-assembly should be generated by ultrasonic nebulization or spraying through nozzle. The size of the droplets thus is limited to a certain range due to the fixed value of ultrasonic frequency of nebulizer, or the nozzle may clog due to aggregation of the precursor materials. Moreover, the particulate materials can be deposited to the inner wall of the furnace of pyrolysis reactor. On the contrary, the bulk synthesis of porous graphene particles is possible with a tunable size range with our emulsion-assisted self-assembly scheme, since nozzles or pyrolysis process are not necessary for the generation and evaporation of the droplets.

The porous graphene microparticles containing titania nanoparticles displayed in Fig. 2(c) were applied as photocatalysts for the decomposition reaction of methylene blue dissolved in water. By fixing the concentration of the organic contaminant as 0.02 g/ dm^3, the initial dose of the photocatalysts in the reaction medium was changed from 0.1 to 0.5 g/dm^3 to study the change of methylene blue concentration as a function of UV irradiation time. As displayed in the graph of Fig. 3(a), the dimensionless concentration (C/C_0) of methylene blue was reduced due to the increase of hydroxyl radicals as the UV irradiation time increased. However, the concentration of methylene blue (C) could not be changed as a function of the UV irradiation time, when the dispersion of graphene nanosheets was adopted as photocatalysts, implying that graphene itself does not have photocatalytic activity. Since the electron-hole pairs are required for the generation of hydroxyl radicals

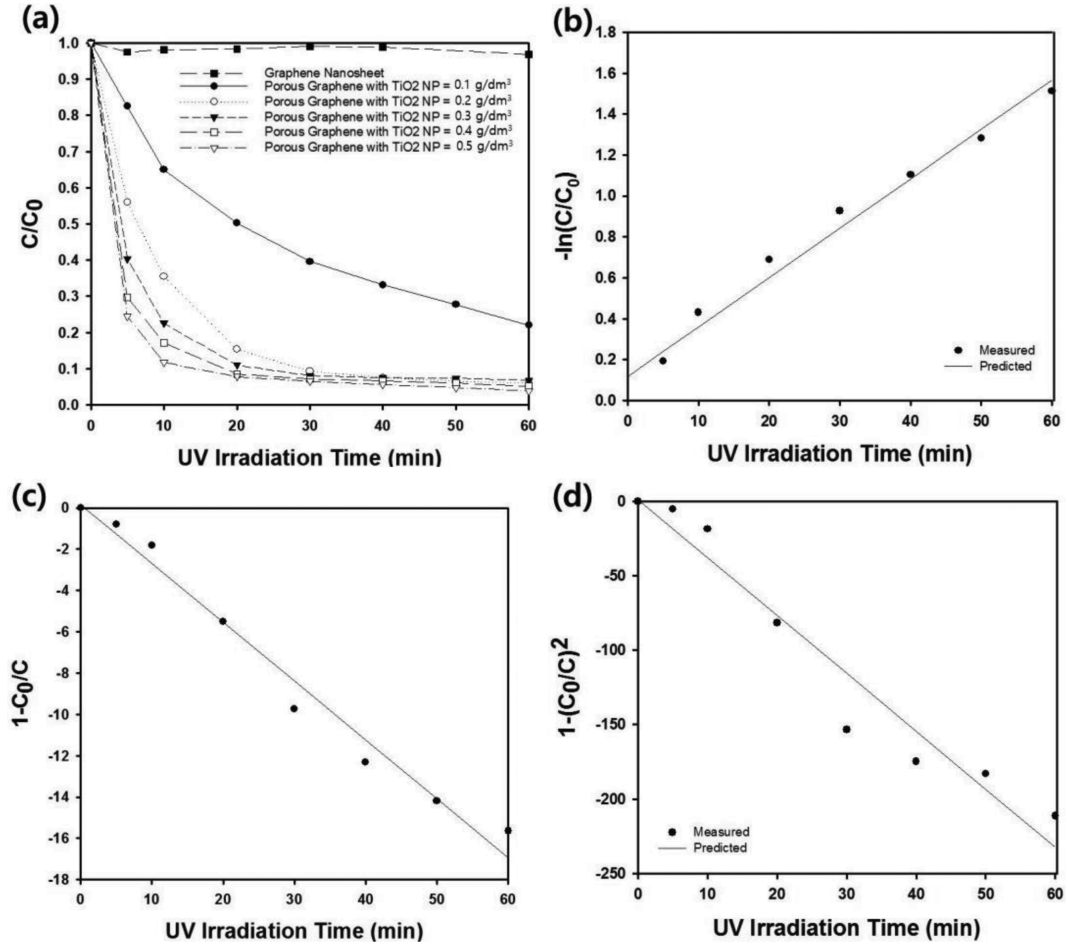


Fig. 3. (a) The change of the dimensionless concentration (C/C_0) of methylene blue as a function of UV irradiation time. The porous graphene microparticles containing titania nanoparticles in Fig. 2(a) were used as a photocatalyst, and the concentration of the photocatalyst for test experiments was 0.1, 0.2, 0.3, 0.4, and 0.5 g/$(dm)^3$. (b) A semi-log plot of the dimensionless concentration as a function of UV irradiation time. The concentration of the photocatalyst was 0.1 g/$(dm)^3$. (c) The change of $(1-C_0/C)$ as a function of UV irradiation time. The concentration of the photocatalyst was 0.2 g/$(dm)^3$. (d) The change of $(1-C_0/C)^2$ as a function of UV irradiation time. The concentration of the photocatalyst was 0.3 g/$(dm)^3$.

from water for the removal of organic pollutants, the introduction of the graphene dispersion without titania could not affect the change of the concentration of methylene blue.

As can be confirmed from Fig. 3(a), the reduction rate of the concentration of the contaminants increased as the amount of the photocatalyst increased, since the number density of hydroxyl radicals generated by the photocatalyst to decompose the organic contaminants increased by increasing the amount of the photocatalyst. When the concentration of the photocatalyst was 0.5 g/dm^3, the half-life ($t_{1/2}$) of the decomposition reaction was just a few minutes, implying that the removal rate of the contaminants increased drastically by the addition of the porous graphene materials in the reaction system. The enhancement of the photocatalytic decomposition rates using the porous graphene structure can be explained by the prolonged lifetime of the electron-hole pairs derived from titania nanoparticles, which increases the generation rates of the hydroxyl radicals for the removal of the pollutants dissolved in water [32]. The porous structure also will be beneficial for the enhancement of the reaction rates since the attachment of the titania nanoparticles will be improved on the porous graphene microparticles as supporting materials. Thus, our-emulsion-assisted self-assembly scheme for the generation of the porous graphene structure could provide an efficient platform for the industrialization of photocatalysts for water purification or air cleaning.

Fig. 3(b) presents a semi-log plot of methylene blue concentration ($-\ln(C/C_0)$) as a function of UV irradiation time when the amount of the photocatalyst was 0.1 g/dm^3 to determine the rate constant of the decomposition reaction. The rate constant could be estimated from the slope of the regression line in Fig. 3(b), assuming that the decomposition reaction is governed by the following first-order reaction.

$$\frac{dC}{dt} = -kC \tag{1}$$

The rate constant k can be predicted from the following equation, which was obtained by taking the natural log to Eq. (1):

$$-\ln\left(\frac{C}{C_0}\right) = kt \tag{2}$$

The estimated rate constant was 0.0242 min^{-1}, whereas the same amount of pure titania nanoparticles resulted in a rate constant of 0.0338 min^{-1}, although detailed experimental data are not reproduced here. However, the mass of the titania nanoparticles contained in the porous graphene microparticles was smaller than the weight of the pure titania nanoparticles, indicating that further addition of the porous photocatalyst may cause more rapid decomposition of methylene blue.

The photocatalytic decomposition reaction can be mainly interpreted according to the first-order kinetics delineated in Eq. (1), which is the special case of Langmuir-Hinshelwood kinetics when the concentration of reactant is small. In our previous research, the rate constants also could be estimated by the first-order kinetics, which could be enhanced by controlling the microstructure of the porous architecture of titania material [33-35]. On the contrary, the first-order kinetics could not be applied to the reaction system in this study, when the amount of the photocatalyst was increased to 0.2 g/dm^3. Under these experimental conditions, the linear regression from the semi-log plot using Eq. (2) was not accurate, whereas the second-order kinetics resulted in better fitting of the experimental data using the following rate equations:

$$\frac{dC}{dt} = -kC^2 \tag{3}$$

$$1 - \frac{C}{C_0} = -kC_0t \tag{4}$$

Fig. 3(c) presents the change of $(1-C_0/C)$ as a function of UV irradiation time, and the second-order rate constant k could be estimated as 1.2683×10^6 mL/(mol·min) from the slope of the regression line in the graph. Thus, the change of reaction order from 1 to 2 corresponded to an increase of the catalyst concentration from 0.1 to 0.2 g/dm^3. This may have been caused by the drastic decrease of the recombination of electron-hole pairs generated from titania during UV irradiation due to the increased amount of graphene. Interestingly, this trend could be also observed when the amount of the photocatalyst increased to 0.3 g/dm^3, which caused the reaction kinetics to follow a third-order reaction according to the following rate equations:

$$\frac{dC}{dt} = -kC^3 \tag{5}$$

$$1 - \left(\frac{C}{C_0}\right)^2 = -2kC_0^2t \tag{6}$$

When the concentration of the photocatalyst was 0.3 g/dm^3, the second-order kinetics was not accurate and linear regression from the graph of $(1-C_0/C)$ vs t was not possible. Fig. 3(d) contains the change of $(1-(C_0/C)^2)$ as a function of UV irradiation time, and the third-order rate constant k could be estimated as 4.63×10^{15} $(mL)^2/(g^2\cdot min)$ from the slope of the regression line in the graph, as summarized in Table 1. As the amount of the photocatalyst increased to 0.4 or 0.5 g/dm^3, the third-order reaction rather than higher order reaction could be better fitted from the experimental data in Fig. 3(a). Although the regression graphs were not reproduced here, the third-order rate constants estimated from the plot

Table 1. The rate constant of the decomposition reaction of methylene blue under UV irradiation by porous graphene microspheres containing titania nanoparticles shown in Fig. 2(c)

The amount of photocatalyst	0.1 g/(dm)^3	0.2 g/(dm)^3	0.3 g/(dm)^3	0.4 g/(dm)^3	0.5 g/(dm)^3
Reaction order	First order	Second order	Third order	Third order	Third order
k	0.0242 min^{-1}	1.2683×10^6 mL/(mol·min)	4.63×10^{15} $(mL)^2/(mol^2\cdot min)$	6.156×10^{15} $(mL)^2/(mol^2\cdot min)$	1.0883×10^{16} $(mL)^2/(mol^2\cdot min)$

of $(1-(C_0/C)^2)$ vs t are summarized in Table 1, when the amount of the photocatalyst was 0.4 or 0.5 g/dm^3. In this study, an increase of the third-order rate constant was observed with an increasing amount of the photocatalyst, as displayed in Fig. 4(a). In summary, the reaction order was not changed when the concentration of the photocatalyst was higher than 0.3 g/dm^3, where the measured third-

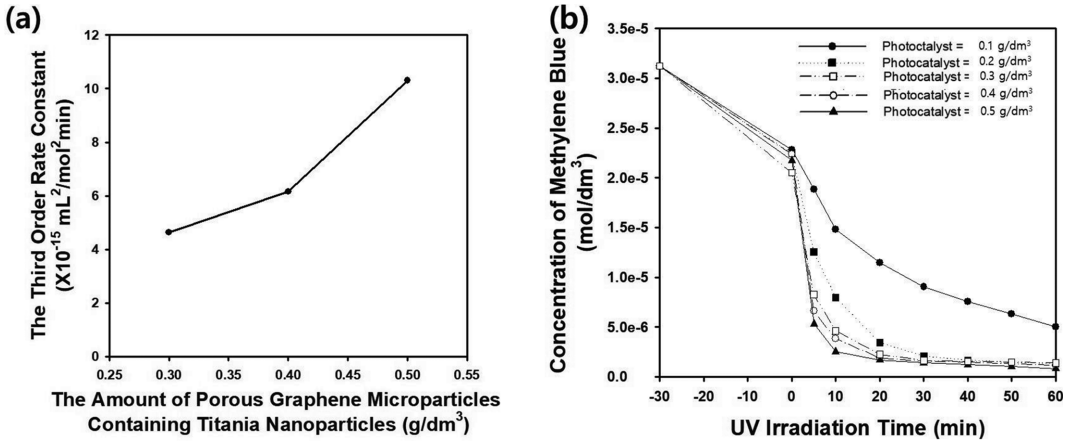


Fig. 4. (a) The change of the third-order rate constant as a function of the amount of porous graphene microparticles containing titania nanoparticles. (b) Concentration change of methylene blue as a function of UV irradiation time. Porous graphene microparticles containing TiO_2 nanoparticles were adopted as photocatalytic particles.

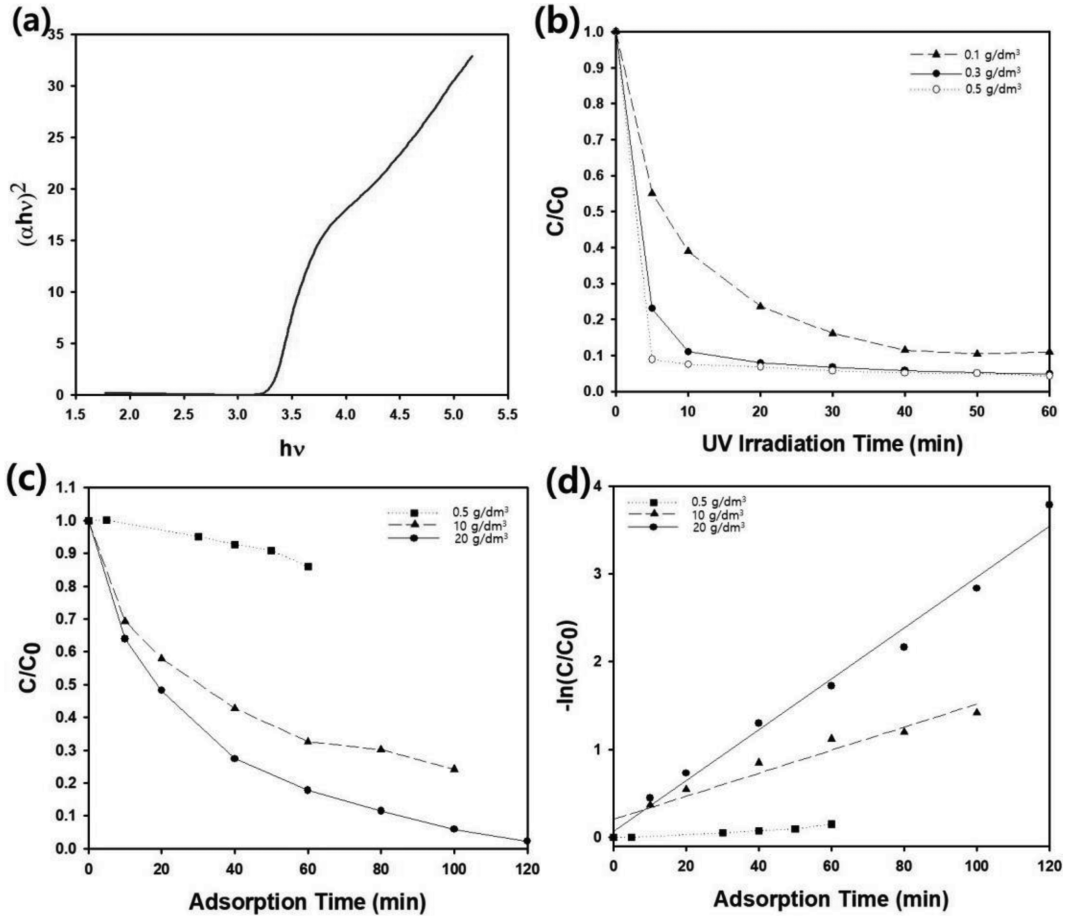


Fig. 5. (a) $(\alpha hv)^2$ as a function of hv obtained from UV-visible diffuse reflectance spectra of porous graphene microparticles containing TiO_2 nanoparticles for band gap evaluation. The change of methylene blue concentration as a function of (b) UV irradiation time and (c) adsorption time, respectively. (d) A semi-log plot of the dimensionless concentration as a function of adsorption time. The porous graphene microparticles containing titania nanoparticles in Fig. 2(e) were used for wastewater treatment.

order rate constant increased with an increasing amount of the photocatalyst.

Before UV illumination, dark condition for 30 minutes was maintained before photocatalytic decomposition of methylene blue. During this equilibration period for 30 minutes, concentration decrease of the dye molecules was observed as contained in the graph of Fig. 4(b). It is thought that adsorption of methylene blue on surface of titania nanoparticles resulted in slight decrease of the dye concentration for 30 minutes without UV irradiation. However, the effect of adsorption was not very significant, indicating that graphene may not be a strong adsorbent of methylene blue molecules.

A change of the reaction order was rarely observed from the photocatalytic decomposition reactions in our previous results using porous titania particles. However, the introduction of graphene materials to the porous photocatalysts resulted in unconventional reaction kinetics such as the second- or third-order reactions, implying that the reaction order can be enhanced remarkably to reduce the required time for completion of the reaction. Thus, the results in this article using porous graphene structures will facilitate industrial applications of photocatalysts in a practical manner.

2. The Kinetics of Methylene Blue Removal using Porous Graphene Microparticles Containing Titania Nanoparticles as Adsorbent

The porous graphene microparticles containing titania nanoparticles shown in Fig. 2(e) were used as a photocatalyst for the decomposition of methylene blue in an aqueous medium. To determine the bandgap energy of the composite microparticles, diffuse reflectance spectrum of the film composed of the microparticles was measured to convert the spectrum to the plot of $(\alpha h\nu)^2$ versus hv shown in Fig. 5(a). From the intercept of abscissa of the graph, the bandgap of the composite microparticles was estimated as about 3.2 eV, which is a similar value of the bandgap of anatase titania. Thus, visible light photocatalysis of the composite microparticles was considered as less efficient manner compared to UV light, since smaller bandgap corresponding to the energy of visible light is required for visible light photocatalysis.

In this study, 10 UV lamps were also used as light source to compare the results obtained using the porous graphene microparticles containing titania nanoparticles shown in the SEM image of Fig. 2(e). Fig. 5(b) displays the resulting values of the dimensionless concentration, C/C_0, as a function of the UV irradiation time for different amounts of photocatalyst. When a relatively high concentration of photocatalyst such as 0.5 g/dm^3 was dissolved in the reaction system, the reducing rate of methylene blue concentration was very fast. This indicates that an increased amount of titania nanoparticles during the synthesis of porous photocatalyst enhanced the reaction rate of methylene blue decomposition.

The porous graphene microparticles containing titania nanoparticles in the SEM image of Fig. 2(e) were also adopted as adsorbent under visible light irradiation for the decomposition reaction of methylene blue, since the bandgap of the composite microparticles was determined as a similar value of anatase titania. Fig. 5(c) presents the resulting graph of C/C_0 as a function of adsorption time. The removal rate of the model contaminant was found to be highly dependent on the concentration of the composite microparticles. For instance, a much higher concentration of the porous graphene microparticles with TiO_2 nanoparticles (20 g/dm^3) was essential to remove most of the methylene blue in the aqueous medium, compared to the necessary amount of the same photocatalyst under UV irradiation (0.5 g/dm^3). However, most of the contaminant could be removed from water, although a relatively concentrated suspension of the adsorbent particles was required in the reaction system. From the regression lines of the semi-log plot shown in the graph of Fig. 5(d), the rate constant of the methy-

Table 2. The rate constant of the adsorption reaction of methylene blue under visible light irradiation by porous graphene microspheres containing titania nanoparticles shown in Fig. 2(e)

The amount of adsorbent	0.5 g/(dm)^3	10 g/(dm)^3	20 g/(dm)^3
k	0.0024 min^{-1}	0.0131 min^{-1}	0.0289 min^{-1}

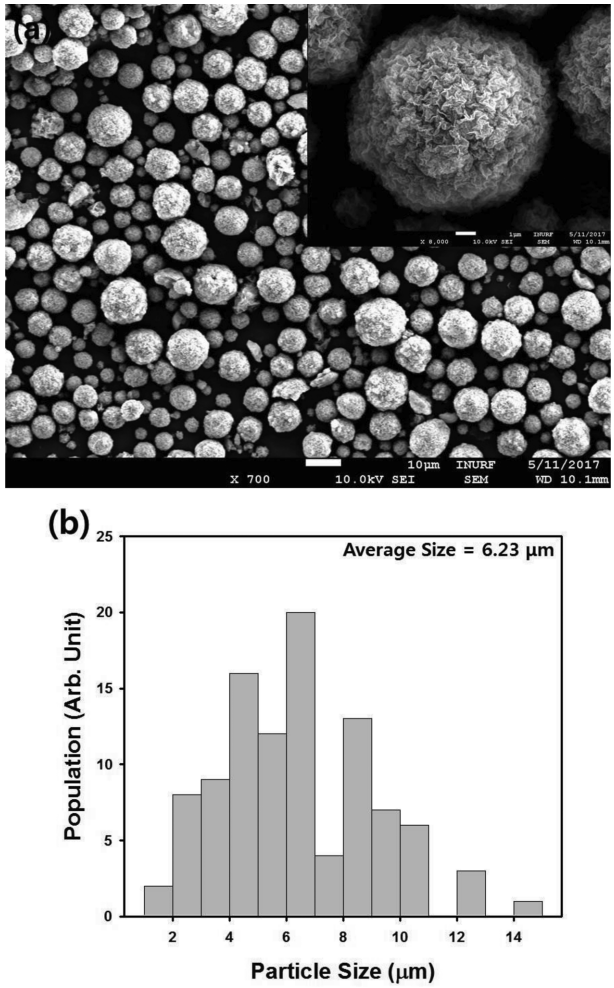


Fig. 6. (a) Scanning electron microscope image of the porous graphene-silica microparticles containing titania nanoparticles. Scale bar indicates 10 μm. The inset figure shows a magnified SEM image of the porous graphene-silica microparticles containing titania nanoparticles. Scale bar is 1 μm. (b) The particle size distribution of the composite microparticles.

lene blue removal could be estimated, and the results are summarized in Table 2. In this study, the maximum rate constant was measured as 0.0289 min^{-1} under the assumption that the first-order reaction kinetics can be adopted, when a sufficient amount of the composite microparticles was suspended in the reaction medium. Here, the value of the rate constant is comparable to the first-order rate constant shown in Table 1, indicating that the porous graphene microparticles with TiO_2 nanoparticles can be adopted as a practical adsorbent as concentrated condition without UV light.

3. The Adsorption and Decomposition of Methylene Blue using Porous Graphene-silica Microparticles Containing Titania Nanoparticles as a Photocatalyst

Porous graphene-silica microparticles containing titania nanoparticles were also synthesized to study the effect of composite structures on the photocatalytic decomposition of methylene blue. Fig. 6(a) contains a scanning electron microscope image of the porous graphene-silica microparticles containing titania nanoparticles fabricated using emulsion droplets as micro-reactors. The surface microstructure of the porous graphene-silica microparticles containing titania nanoparticles displayed in the inset SEM image of Fig. 6(a) shows rougher morphologies compared to the result in Fig. 2, since the addition of silica precursor like silicic acid resulted in the formation of additional rough micro-domains in the composite particles. The particle size distribution was obtained by measuring the diameter of several particles from a low magnification SEM image, and the results are plotted in Fig. 6(b). The average diameter of the porous particles was estimated as 6.23 μm, which is slightly larger than the result from the porous graphene microparticles containing titania nanoparticles. Since the addition of the silica precursor to the dispersed phase caused a slight increase of the precursor concentration inside the droplets, the particle diameter became larger for porous graphene-silica microparticles containing titania nanoparticles.

Table 3. XPS analysis results of graphene-TiO_2 and silica-graphene-TiO_2 microparticles

Element	C	O	Si	Ti
Graphene-TiO_2	32.85	49.47	-	17.67
Silica-graphene-TiO_2	40.82	44.62	13.78	0.78

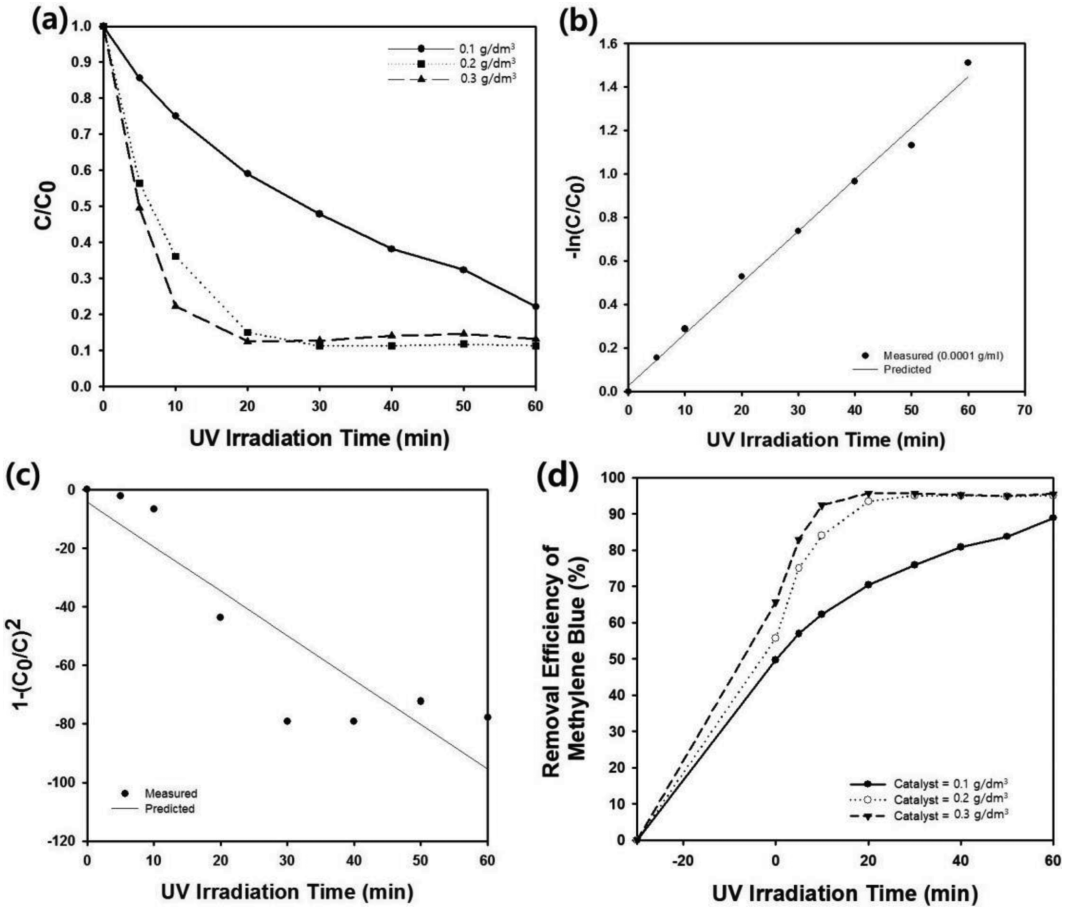


Fig. 7. (a) The change of the dimensionless concentration (C/C_0) of methylene blue as a function of UV irradiation time. The porous graphene-silica microparticles containing titania nanoparticles shown in Fig. 5(a) were used as a photocatalyst, and the concentration of the photocatalyst for the test experiments was 0.1, 0.2, and 0.3 g/$(dm)^3$. (b) A semi-log plot of the dimensionless concentration. The concentration of the photocatalyst was 0.1 g/$(dm)^3$. (c) The change of $(1-C_0/C)^2$ as a function of UV irradiation time. The concentration of the photocatalyst was 0.2 g/$(dm)^3$. (d) Removal efficiency of methylene blue as a function of UV irradiation time. Before UV irradiation, dark condition for 30 minutes was also included in the graph.

The composition of graphene-silica microparticles containing TiO_2 nanoparticles was confirmed by XPS analysis, as displayed in Table 3. For comparison, XPS analysis result of graphene-TiO_2 microparticles were also included in the table, indicating that significant amounts of Si and O element were confirmed by the addition of silicic acid inside dispersed phase during synthesis of graphene-silica-TiO_2 microparticles. However, reduction of the amount of Ti element has been observed in graphene-silica-TiO_2 microparticles, implying that penetration of incident beam to the sample during XPS analysis might become difficult, since TiO_2 nanoparticles could be coated inside the silica matrix.

The photocatalytic performance of the porous graphene-silica microparticles containing TiO_2 nanoparticles is summarized in the graphs of Fig. 7. The change of methylene blue concentration is displayed in Fig. 7(a) as a function of the UV irradiation time according to the amount of photocatalyst in the reaction system. As the decomposition time increased, the dimensionless concentration of the contaminant (C/C_0) decreased in a similar pattern to that of Fig. 3(a). When the concentration of the porous graphene-silica microparticles containing titania nanoparticles was 0.1 g/dm^3, the first-order reaction kinetics could be applied and the regression line was well fitted with the semi-log plot in Fig. 7(b). The estimated rate constant using Eq. (2) was 0.0237 min^{-1}, which is similar to the first-order rate constant of the porous graphene microparticles containing titania nanoparticles. When the amount of the photocatalyst was increased to 0.2 g/dm^3, the third-order kinetics was more accurate than the second-order kinetics to fit the experimental data. The change of $(1-(C_0/C)^2)$ is plotted as a function of the UV irradiation time in Fig. 7(c) to determine the third-order

Table 4. The rate constant of the decomposition reaction of methylene blue under UV irradiation by porous graphene-silica microspheres containing titania nanoparticles shown in Fig. 6(a)

The amount of photocatalyst	0.1 g/(dm)^3	0.2 g/(dm)^3
Reaction order	First order	Third order
k	0.0237 min^{-1}	3.965×10^{16} (mL)^2/(mol^2·min)

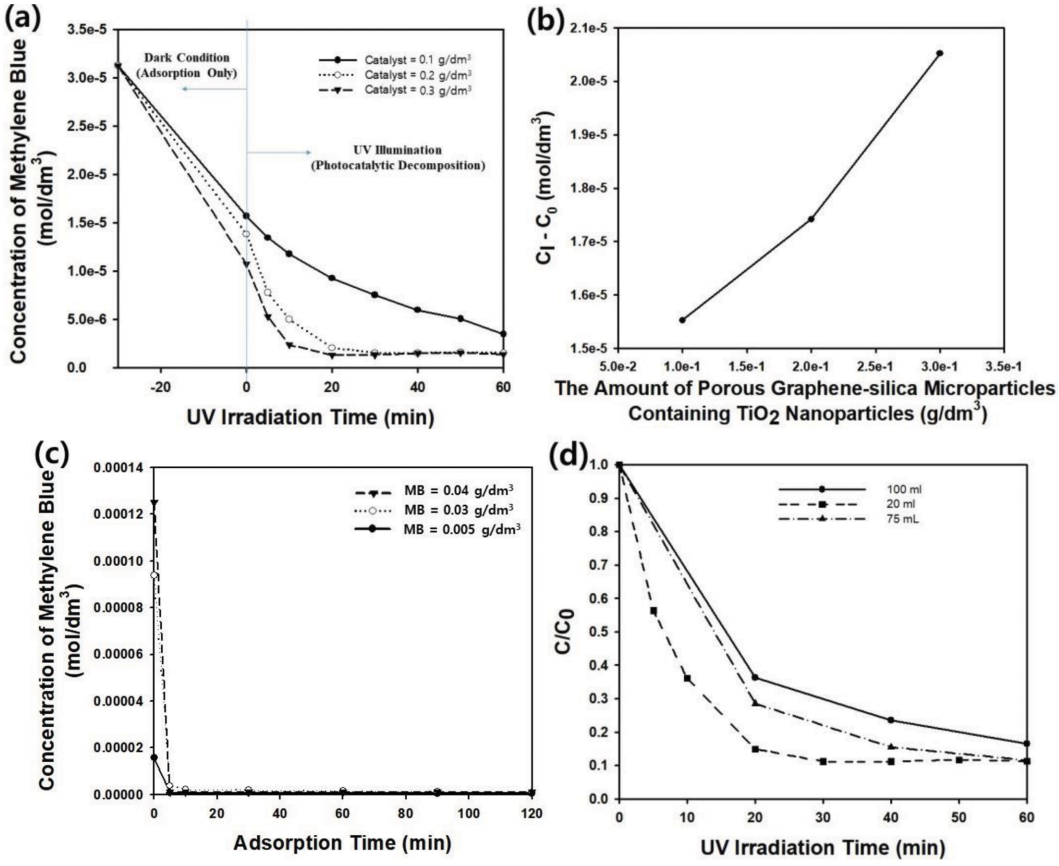


Fig. 8. (a) The change of methylene blue concentration as a function of UV irradiation time. The data during a dark condition for 30 minutes before UV illumination were also included in the graph. Porous graphene-silica microparticles containing titania nanoparticles shown in Fig. 5(a) were used as a photocatalyst. (b) $C_I - C_0$ as a function of the amount of the photocatalyst. (c) Concentration change of methylene blue as a function of adsorption time. Porous graphene-silica microparticles without titania particles were used as adsorbent particles. Initial dose of methylene blue was adjusted from 0.005 to 0.03 g/(dm)^3 for each experiment. For (a), (b), and (c), the volume of reactant was 20 ml. (d) Change of dimensionless concentration of methylene blue as a function of UV irradiation time. Porous graphene-silica microparticles containing titania nanoparticles shown in Fig. 5(a) were used as a photocatalyst. Photocatalytic decomposition was carried in batch-mode reactor with total volume of 20, 75, and 100 ml.

rate constant from the slope of the regression line, which was estimated as 3.965×10^{16} $(mL)^2/(mol^2\cdot min)$, as summarized in Table 4.

Fig. 7(d) contains the removal efficiency of methylene blue as a function of UV irradiation time using porous graphene-silica-TiO_2 particles as photocatalytic material. When the concentration of the photocatalytic particles was 0.2 or 0.3 g/dm^3, more than 95% of the organic dye could be removed by adsorption and photocatalytic decomposition after 60 minutes of UV illumination.

A hydrophilic pollutant such as methylene blue dissolved in an aqueous medium may also be physically adsorbed on a hydrophilic surface composed of silica. Thus, it can be expected that the porous graphene-silica microparticles containing titania nanoparticles may adsorb methylene blue, and the organic contaminants in water can be decomposed simultaneously after UV irradiation. To confirm this hypothesis, the concentration of methylene blue before UV irradiation (−30 minutes) was plotted with the experimental data during photocatalytic decomposition (after 0 to 60 minutes). Although a composite of activated carbon and titania has been employed for adsorption and decomposition of dye molecules under UV illumination, we have tried to apply our own micro-structured materials such as the graphene-silica-TiO_2 composite microparticles displayed in Fig. 6(a) [36]. Fig. 8(a) presents the change of the concentration of methylene blue as a function of elapsed time, which can be divided into the time for physical adsorption in a dark condition (30 minutes) and the photocatalytic decomposition time during UV irradiation (60 minutes). During the physical adsorption, external light was blocked to avoid photocatalytic decomposition of the contaminant. When UV illumination started, the concentration of methylene blue (C_0) became smaller than the initial dose of methylene blue (C_I=0.02 g/dm^3). As displayed in the graph of Fig. 8(b), the difference between C_I and C_0 increased as the amount of the photocatalyst increased. This indicates that the amount of the methylene blue adsorbed physically on the photocatalyst was proportional to the amount of porous microparticles in the slurry-type photocatalytic reactor. Assuming that the rate of adsorption is governed by the first-order kinetics, the rate constant for adsorption was calculated for three different amounts of the photocatalyst, and the estimated values are summarized in Table 5. For instance, the first-order rate constant was estimated as 0.0237 and 0.0229 min^{-1} for chemical decomposition and physical adsorption, respectively, when the amount of the photocatalyst was 0.1 g/dm^3. Although the rate constant of adsorption is slightly smaller than that of the photocatalytic decomposition reaction, it can be concluded that a significant amount of methylene blue was adsorbed on the surface of porous graphene-silica microparticles containing titania nanoparticles before the illumination of UV light to the reaction system.

The physical adsorption of methylene blue could be more clearly confirmed from adsorption kinetics data shown in Fig. 8(c), which was obtained using porous graphene-silica microparticles synthesized without using titania nanoparticles. Compared to the experimental result shown in Fig. 8(a), the excess adsorbent particles were used (1 g/dm^3) for complete removal of the dye molecules by adsorption. In this case, small amount of methylene blue (0.005 to 0.3 g/dm^3) added to the adsorber could be removed completely within a few minutes, as displayed in the graph of Fig. 8(c).

Methylene blue was removed using graphene-silica microparticles containing TiO_2 nanoparticles by changing the volume of reactants in batch photocatalytic reactor. As shown in the graph of Fig. 8(d), decreasing rate of the dye concentration became slower as the volume of the reactant increased from 20 to 100 ml, since

Table 5. The adsorption rate constant of methylene blue by porous graphene-silica microspheres containing titania nanoparticles shown in Fig. 6(a)

The amount of photocatalyst	0.1 g/(dm)^3	0.2 g/(dm)^3	0.3 g/(dm)^3
k	0.0229 min^{-1}	0.027251 min^{-1}	0.0356 min^{-1}

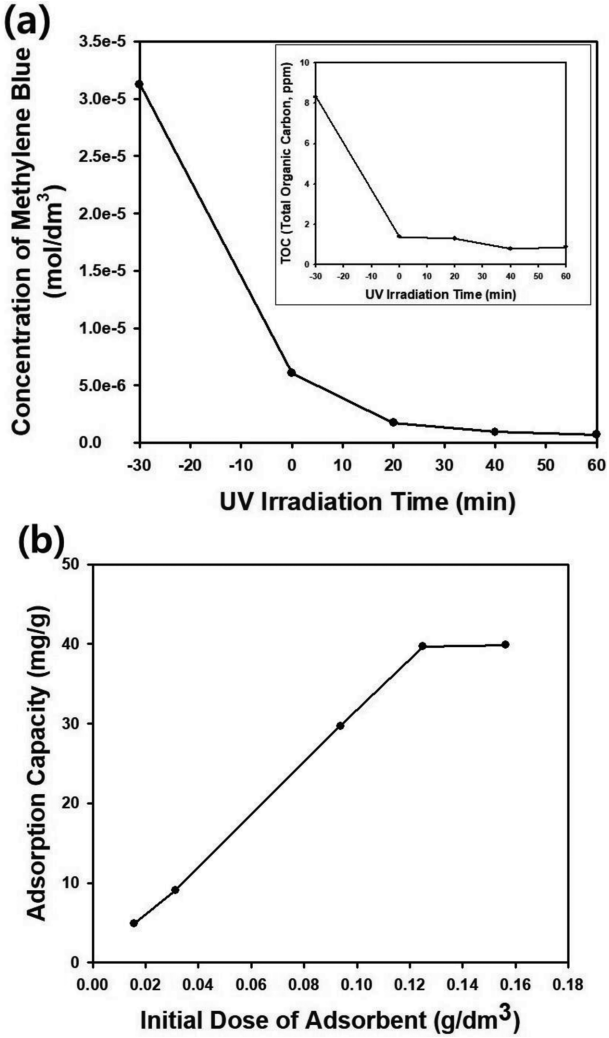


Fig. 9. (a) Change of methylene blue concentration as a function of UV irradiation time. The volume of reactant was maintained as 75 ml, and porous graphene-silica microparticles containing TiO_2 nanoparticles were used as photocatalyst. Inset graph contains the change of TOC as a function of time. (b) Adsorption capacity of porous graphene-silica microparticles containing TiO_2 nanoparticles during removal of methylene blue as a function of initial dose of the adsorbent particles. Concentration of adsorbent particles was fixed as 1 g/dm^3.

the amount of dye molecules for decomposition increased under fixed UV irradiation power using 8 UV lamps. However, the concentration of methylene blue after 60 minutes of UV irradiation was measured as similar values for the sample with reactor volume of 20 and 75 ml, indicating that removal of chromacity from wastewater is possible after adequate scale-up of the photocatalytic system without increasing UV irradiation power.

Fig. 9(a) contains change of methylene blue concentration as a function of UV irradiation time when porous graphene-silica microparticles containing TiO_2 nanoparticles were adopted as photocatalyst in 75-ml aqueous reactant. As displayed in the graph, significant amount of methylene blue could be removed by adsorption mechanism during equilibration at dark condition for 30 minutes, and successive removal of the remaining dyes was possible by photocatalytic decomposition for 60 minutes of UV irradiation. Since the concentration was measured using absorbance at characteristic peak wavelength from UV-visible spectrum, additional TOC (total organic carbon) analyses were carried out for the same samples. The inset graph in Fig. 9(a) shows the change of TOC as a function of UV irradiation time, indicating that similar decreasing trend as the results from UV-visible spectrum was observed during adsorption and photocatalytic decomposition stage. However, the decrease of TOC during UV irradiation was not as significant as that of dye concentration (C/C_0), implying that most organic materials could be removed by adsorption mechanism, whereas the chromophore group of methylene blue could be dissociated by photocatalytic decomposition. pH of the aqueous solution was recorded as 6.41 before equilibration at dark condition and maintained in the range from 6.39 to 6.4 during UV irradiation, indicating that the pH value of aqueous solution containing model contaminant and particulate materials was similar to distilled water.

Since wastewater from dye factory cannot be recycled for industrial purposes due to their color, photocatalytic degradation to decompose chromophore groups of dye molecules can be considered effective. However, additional removal mechanism is necessary, since photocatalytic mechanism may not be sufficient to remove organic contaminants dissolved in aqueous medium completely. Thus, our porous microparticles having synergetic functionality of adsorption ability and photocatalytic activity can be applied to a wastewater treatment system including organic pollutants such as dye molecules. Since most researches have focused on adsorption and photocatalytic degradation separately, it may be advantageous to develop functional microparticles having both mechanisms simultaneously. In this study, we have developed microparticles having both functionality of adsorption and photocatalytic activity, as displayed in Fig. 9(a).

To estimate adsorption efficiency of porous silica-graphene microparticles containing TiO_2 nanoparticles, adsorption capacity of the adsorbent during removal of methylene blue was measured as a function of the initial dose of the adsorbent particles, as shown in Fig. 9(b). Initial linear dependence of adsorption capacity became saturated after addition of excess adsorbent particles, and the maximum adsorption capacity of the composite microparticles can be estimated as about 40 mg/g (mass of methylene blue per mass of adsorbent particles), which was comparable to that of activated

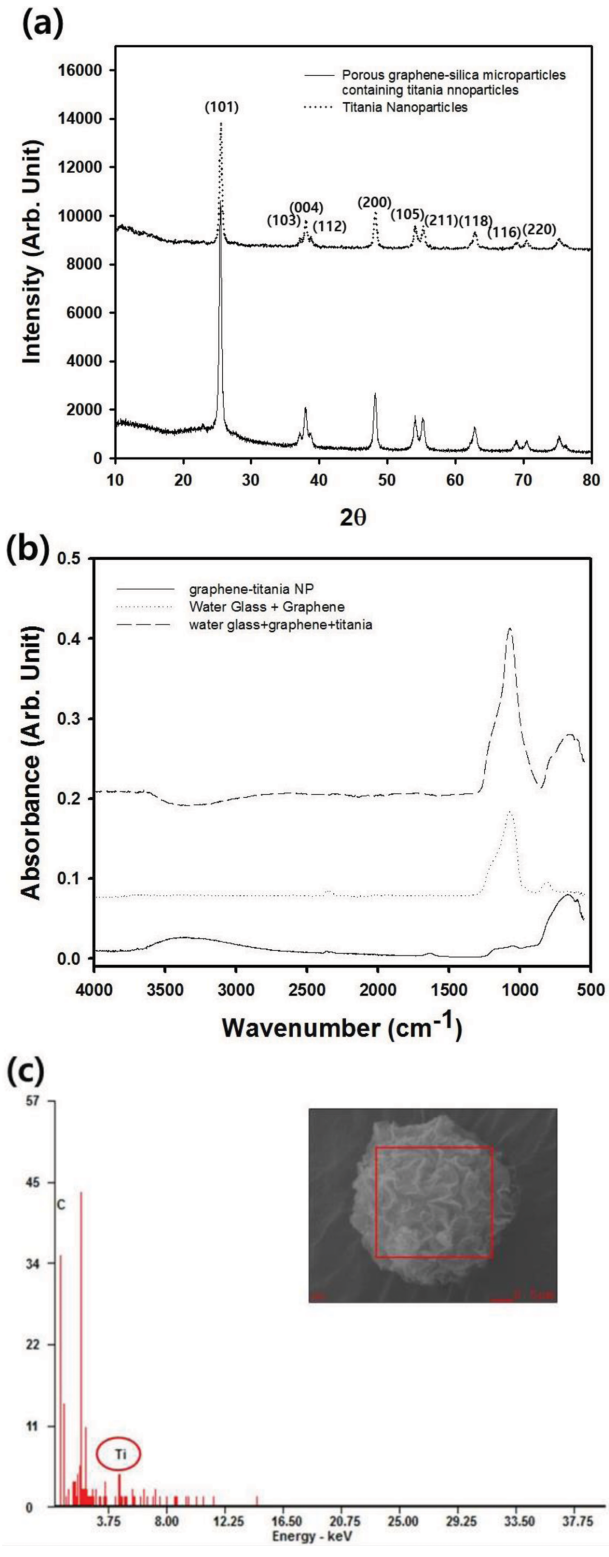


Fig. 10. (a) Powder XRD analysis results of porous graphene-silica microparticles containing titania nanoparticles and pure titania nanoparticles. (b) FT-IR spectrum of the porous graphene or graphene-silica microparticles containing titania nanoparticles. For comparison, the spectrum of the porous graphene-silica microparticles was included in the same plot. (c) EDS result of the porous graphene microparticles containing titania nanoparticles.

carbon, implying that our composite microparticles can be applied as excellent adsorbent as well as photocatalytic particles [37].

Fig. 10(a) presents the powder XRD analysis results of pure titania nanoparticles and porous graphene-silica microparticles containing titania nanoparticles. The characteristic peaks originating from graphene and silica could not be observed from the XRD results, and the diffraction peaks from anatase titania were observed, since the XRD results of pure titania nanoparticles and porous graphene-silica microparticles containing titania nanoparticles coincided well with each other. Thus, the existence of graphene and titania nanoparticles attached to the porous graphene microparticles with or without titania nanoparticles was confirmed from FT-IR spectrum of the sample, as displayed in the graph of Fig. 10(b). For porous graphene-silica microparticles without titania nanoparticles, the characteristic peak appeared at 800 cm^{-1} due to the vibration of Si-O bond, implying that silicon dioxide could be synthesized from the silicic acid precursor [38]. Although the results are not reproduced here, the characteristic peaks that appeared at 621, 594, and 549 cm^{-1} originating from Ti-O vibrations could be confirmed from the titania nanoparticles by the FT-IR spectrophotometer observations [39]. Similar peaks were also observed from the porous graphene microparticles containing titania nanoparticles and the porous graphene-silica microparticles containing titania nanoparticles, implying that the physical binding of titania was successful for both types of porous photocatalysts. Since the characteristic peaks of FT-IR spectra originating from TiO_2 nanoparticles and silica are quite different, we could detect the existence of silica matrix from porous graphene-silica microparticles containing TiO_2 nanoparticles. In Fig. 10(b), the characteristic peaks of TiO_2 nanoparticles and silica were observed together, indicating that composite microparticles of silica and TiO_2 could be synthesized from emulsion droplets as micro-reactors.

Besides the peaks due to titania, the absorption peak at 1,643 cm^{-1} that originated from C=C bonds in the graphene nanosheets was also detected, indicating that the porous graphene microparticles containing titania nanoparticles were successfully prepared by emulsion-assisted self-assembly [40]. In addition to the results of XRD and FT-IR analyses, the existence of elemental titanium was confirmed by an EDS analysis for the porous graphene microparticles containing titania nanoparticles. As displayed in Fig. 10(c), the main component of the porous particles was found to be carbon, which was derived from the graphene nanosheets. However, Ti element was also detected, since a dispersion of titania nanocolloid was used as raw material for the fabrication of the photocatalytic particles. Thus, the existence of graphene and silica of porous graphene-silica microparticles containing TiO_2 nanoparticles could be detected by FT-IR and EDS analysis.

The morphology of graphene-silica microparticles containing TiO_2 nanoparticles was observed by transmission electron microscope, as displayed in Fig. 11. From the edge of the composite microparticles, thin nanosheets can be observed in the image of Fig. 11(a), which can be considered as graphene nanosheets added during synthesis. From the magnified TEM image in Fig. 11(b), it was difficult to recognize the detailed morphology in dark part near the central region of the microparticles, since graphene nanosheets are covered with thick layer of silica and TiO_2.

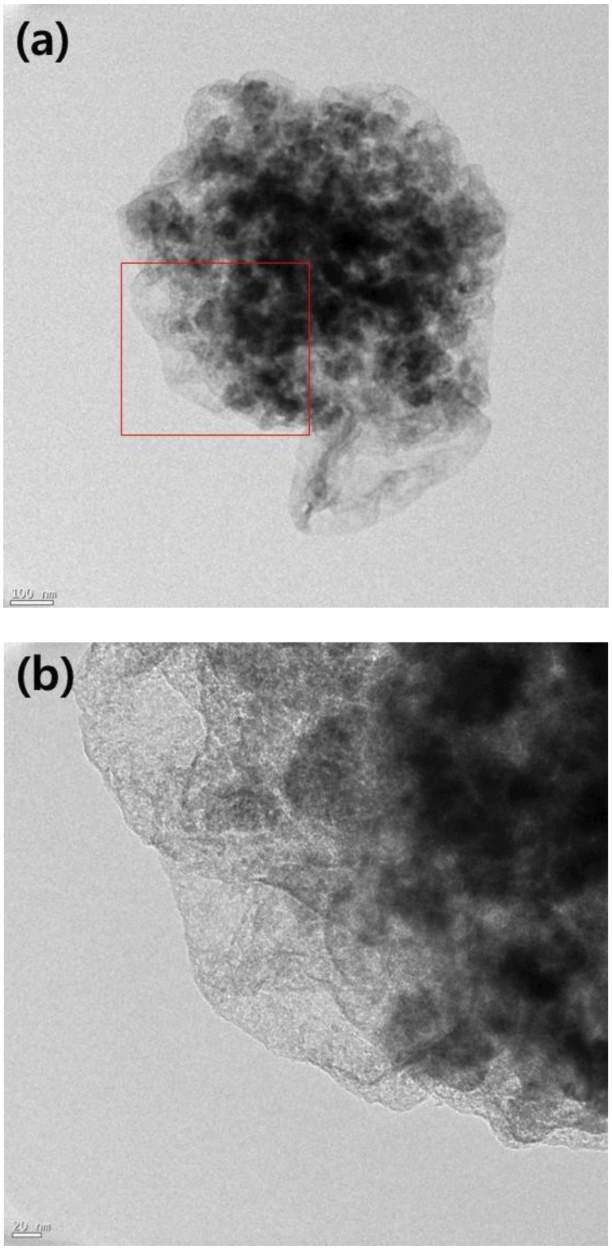


Fig. 11. (a) TEM image of silica-graphene microparticles containing TiO_2 nanoparticles. (b) Magnified TEM image of highlighted region of the image in Fig. 10(a). Scale bar indicates 100 and 20 nm for (a) and (b), respectively.

The kinetics of photocatalytic decomposition in this study could be estimated as the second- or third-order, indicating that very fast decomposition rate occurred due to the porous nature of graphene or graphene-silica microparticles causing adsorption of methylene blue. Though most photocatalytic decomposition reactions can be considered as the first-order kinetics, higher -order kinetics such as the second- or third-order have been also proposed. For instance, photocatalytic degradation of Congo red dye in aqueous medium could be fitted by the second-order kinetics using Fe-chromite under UV light [41]. Similarly, photocatalytic mineralization of sodium dodecylbenzenesulphonate has been also studied as the second-

order kinetics using TiO_2 as photocatalyst [42]. Nd-doped titania has been also adopted for photocatalytic degradation of tri-n-butyl phosphate to study the reaction kinetics as third-order under alkali condition [43]. Thus, the third-order kinetics in this study can be also regarded as possible reaction order during photocatalytic decomposition reaction.

The degradation mechanism of methylene blue by photocatalytic decomposition using titania-based photocatalyst is important to understand photocatalytic oxidation of organic dyes. For this purpose, chemical analyses of reaction intermediate are essential, although such research could not be carried out in this study. However, complex photocatalytic degradation mechanism of methylene blue by TiO_2 has been carried out using GC-MS technique from another research group [44]. According to their results, it has been reported that N-S heterocyclic group of methylene blue can be attacked by hydroxyl radicals generated from TiO_2 and aqueous medium, yielding 2-amino-5-dimethylamino benzenesulfonic acid anion and dimethyl-(4-nitro phenyl) amine. Successive degradation of 2-amino-5-dimethylamino benzenesulfonic acid anion results in the generation of 4-amino benzenesulfonic acid and 2-amino-5-dimethylamino benzenesulfonic acid. After oxidation of 4-amino benzenesulfonic acid, 4-nitro benzenesulfonic acid anion can be formed, followed by degradation into CO_2 and H_2O. Thus, organic dyes can be dissociated as CO_2 and H_2O by photocatalytic mineralization process during wastewater treatment process.

CONCLUSION

Porous graphene and graphene-silica microparticles containing titania nanoparticles were synthesized by emulsion-assisted self-assembly using graphene nanosheets, silicic acid, and titania nanocolloid as precursor materials. An evaporation-driven self-assembly scheme was adopted to prepare the porous particles with a photocatalytic property through self-assembly and high-temperature calcination. The composition of the porous particles was confirmed by FT-IR and XPS analyses to check the carbon materials in the composite particles containing graphene. The final morphologies of the photocatalytic particles were spherically porous microparticles with irregular macropores that were generated from folding and crumpling of the graphene nanosheets inside shrinking emulsion droplets.

As an application of the porous particles, the photocatalytic decomposition of methylene blue in an aqueous medium was carried out using a slurry-type reactor under UV light irradiation. By monitoring the concentration change as a function of the UV irradiation time, the rate constant and the half life of the porous photocatalysts were evaluated depending on the amount of the photocatalyst. When a sufficient amount of the photocatalyst was used in the decomposition reaction, the kinetics was changed from the first-order reaction to the second- or third-order reaction, indicating that Langmuir-Hinshelwood kinetics could not be applied to the reaction system. Thus, extremely fast decomposition rates could be achieved under proper experimental conditions with half-life as short as a few minutes, indicating that the graphene-based photocatalysts are potentially applicable to water purification industries. Since commercialization of photocatalytic materials is limited due to their relatively slower degradation time compared to other purification methods, our porous graphene-silica microparticles with half-life of degradation reaction as only a few minutes will be advantageous to water treatment systems in industries.

The limitation of this study is related to the collection of photocatalytic microparticles after degradation of organic dye molecules. Presently, natural sedimentation of the microparticles under gravitational force is the only choice, though required sedimentation time is within a few hours. Thus, a study on the synthesis of magnetically active photocatalytic particles is underway as future work.

ACKNOWLEDGEMENTS

This research was supported by the Basic Science Research Program through the National Research Foundation of Korea (NRF) funded by the Ministry of Science, ICT & Future Planning (NRF-2017R1C1B5017174), the Priority Research Centers Program through the National Research Foundation of Korea (NRF) funded by the Ministry of Education (NRF-2017R1A6A1A03015562), and Korea Institute for Advancement of Technology (KIAT) grant funded by the Korea Government (MOTIE) (P002007, The Competency Development Program for Industry Specialist).

REFERENCES

1. S. Ould-Chikh, S. Pavan, A. Fecant, E. Trela, C. Verdon, A. Gallard, N. Crozet., J.-L. Loubet, M. Hemati and L. Rouleau, *Stud. Surf. Sci. Catal.*, **175**, 193 (2010).
2. S. Ciampi, T. Böcking, K. A. Kilian, J. B. Harper and J. J. J. Gooding, *Langmuir*, **24**(11), 5888 (2008).
3. C.-F. Wang and L.-T. Chen, *Langmuir*, **33**(8), 1969 (2017).
4. L. Ernawati, T. Ogi, R. Balgis, K. Okuyama, M. Stucki, S. C. Hess and W. J. Stark, *Langmuir*, **32**(1), 338 (2016).
5. Y.-S. Cho, I.-A. Oh and N. R. Jung, *J. Ceram. Processing Res.*, **17**(6), 573 (2016).
6. C. M. Wu and M. H. Chou, *Eur. Polym. J.*, **82**, 35 (2016).
7. L. Passoni, L. Criante, F. Fumagalli, F. Scotognella, G. Lanzani and F. D. Fonzo, *ACS Nano*, **8**(12), 12167 (2014).
8. R. M. Dorin, H. Sai and U. Wiesner, *Chem. Mater.*, **26**(1), 339 (2014).
9. T. Bollhorst, T. Grieb, A. Rosenauer, G. Fuller, M. Maas and K. Rezwan, *Chem. Mater.*, **25**(17), 3464 (2013).
10. A. Fujishima and K. Honda, *Nature*, **238**(5358), 37 (1972).
11. Y.-S. Cho, I.-A. Oh and N. R. Jung, *J. Disper. Sci. Technol.*, **37**, 676 (2016).
12. D. S. Bhachu, S. Sathasivam, C. J. Carmalt and I. P. Parkin, *Langmuir*, **30**(2), 624 (2014).
13. H. Yoo, S. Kahng and J. H. Kim, *Sol. Energ. Mat. Sol. C.*, **204**, 110211 (2020).
14. D. Bak and J. H. Kim, *J. Power Sources*, **389**, 70 (2018).
15. J. Fu, Q. Xu, J. Low, C. Jiang and J. Yu, *Appl. Catal. B.*, **243**, 556 (2019).
16. T. Su, Q. Shao, Z. Qin, Z. Guo and Z. Wu, *ACS Catal.*, **8**, 2253 (2018).
17. Q. Xu, L. Zhang, J. Yu, S. Wageh, A. A. Al-Ghamdi and M. Jaroniec, *Mater. Today*, **21**(10), 1042 (2018).
18. J. Low, B. Dai, T. Tong, C. Jiang and J. Yu, *Adv. Mater.*, **31**(6), 1802981 (2018).
19. B. Lin, H. Li, H. An, W. Hao, J. Wei, Y. Dai, C. Ma and G. Yang,

Appl. Catal. B, **220**, 542 (2018).
20. X. Cai, J. Zhang, M. Fujitsuka and T. Majima, *Appl. Catal. B*, **202**, 191 (2017).
21. Y. Horiguchi, T. Kanda, K. Torigoe, H. Sakai and M. Abe, *Langmuir*, **30**(3), 922 (2014).
22. B. Sun, A. V. Vorontsov and P. G. Smirniotis, *Langmuir*, **19**(8), 3151 (2003).
23. D. B. Hamal, J. A. Haggstrom, G. L. Marchin, M. A. Ikenberry, K. Hohn and K. J. Klabunde, *Langmuir*, **26**(4), 2805 (2010).
24. K. K. Paul, R. Ghosh and P. K. Giri, *Nanotechnology*, **27**, 315703 (2016).
25. V. R. Posa, V. Annavaram, J. R. Koduru, P. Bobbala, V. Madhavi and A. R. Somala, *J. Exp. Nanosci.*, **11**(9), 722 (2016).
26. K. Y. Foo and B. H. Hameed, *Desalin. Water Treat.*, **19**, 255 (2010).
27. G. N. Shah and R. Lemilch, *Ind. Eng. Chem. Fundamentals*, **9**(3), 350 (1970).
28. Y.-S. Cho, N. Ku and Y.-S. Kim, *J. Chem. Eng. Jpn.*, **52**(2), 194 (2019).
29. Y.-S. Cho and S. H. Roh, *J. Disper. Sci. Technol.*, **39**(1), 33 (2018).
30. H. D. Jang, S. K. Kim, H. Chang, J.-W. Choi, J. Luo and J. Huang, *Aerosol Sci. Technol.*, **47**(1), 93 (2013).
31. S.-H. Park, H.-K. Kim, S.-B. Yoon, C.-W. Lee, D. Ahn, S.-I. Lee, K. C. Roh and K.-B. Kim, *Chem. Mater.*, **27**(2), 457 (2015).
32. T.-F. Yeh, J. Cihlar, C.-Y. Chang, C. Cheng and H. Teng, *Mater. Today*, **16**(3), 78 (2013).
33. I.-A. Oh, C. H. Shin and Y.-S. Cho, *Korean J. Met. Mater.*, **54**(8), 573 (2016).
34. Y.-S. Cho and C. H. Shin, *Korean J. Chem. Eng.*, **34**(2), 555 (2017).
35. Y.-S. Cho, *Korean J. Met. Mater.*, **55**(4), 150 (2017).
36. M.-L. Chen, J.-S. Bae and W.-C. Oh, *Bull. Kor. Chem. Soc.*, **27**(9), 1423 (2006).
37. D. Pathania, S. Sharma and P. Singh, *Arab. J. Chem.*, **10**, S1445 (2007).
38. C. Moore, T. S. Perova, B. Kennedy, K. Berwickc, I. L. Shaganov and R. A. Moore, *Proc. SPIE*, **4876**, 1247 (2003).
39. M. Hema, A. Y. Arasi, P. Tailselvi and R. Anbaasan, *Chem. Sci. Trans.*, **2**(1), 239 (2013).
40. S. Sharin, I. A. Rahman, A. F. Ahmad, H. M. K. Mohd, F. Mohamed, F. Radiman, M. S. Yasir, S. Sarmani, M. T. M. Ayob and I. S. Bastamam, *Malays. J. Anal. Sci.*, **19**(6), 1223 (2015).
41. M. Shaban, M. R. Abukhadra, S. S. Ibrahim and M. G. Shahien, *Appl. Water Sci.*, **7**, 4743 (2017).
42. M. Sanchez, M. J. Rivero and I. Ortiz, *Appl. Catal. B*, **101**, 515 (2011).
43. H. G. Mobtaker, A. Malekinejad, T. Yousefi and H. Aghayan, *J. Sci., I. R. I.*, **28**(1), 79 (2017).
44. X. Wang, S.-f. Han, Q.-w. Zhang, N. Zhang and D.-d. Zhao, *MATEC Web of Conferences*, **238**, 03006 (2018).